Size and Structure of Antigen–Antibody Complexes: Thermodynamic Parameters†

Regina M. Murphy,*,‡ Richard A. Chamberlin,§ Peter Schurtenberger,§ Clark K. Colton,‡ and Martin L. Yarmush∥

Departments of Chemical Engineering and Physics and Center for Materials Research, Massachusetts Institute of Technology, Cambridge, Massachusetts 02139, and Department of Chemical and Biochemical Engineering, Rutgers University, Piscataway, New Jersey 08855

Received March 15, 1990; Revised Manuscript Received August 14, 1990

ABSTRACT: The role of antigen–antibody (Ag–Ab) complexes in the immune response depends, in part, on the size of the complexes. Previously, we combined electron microscopy with classical and quasi-elastic light scattering to characterize the molecular weight distribution and the conformation of Ag–Ab complexes made from bovine serum albumin (BSA) and pairs of anti-BSA monoclonal antibodies at a single concentration and Ag:Ab molar ratio. In this report, the molecular weight distribution of Ag–Ab complexes was determined by classical light scattering at a single Ag:Ab ratio and over a range of concentrations, and binding of BSA to pairs of MAb was determined by radioimmunoassay at several Ag:Ab molar ratios. A thermodynamic model was developed for the equilibrium size distribution of Ag–Ab complexes formed between a pair of MAb, each with unique affinity and specificity, and an Ag containing a single epitope for each of the pair of MAb. The combined experimental data were used in conjunction with the model to determine the values of cyclization and polymerization constants. Successful determination of the parameters required data from both classical light scattering and electron microscopy. Cyclization constants were lower than those reported in other studies of Ag–Ab complexes; this may be attributable to our use of a protein Ag, as compared to a divalent hapten. In two out of three cases, cyclization constants increased with increasing number of Ab in the complex, in contrast to previous assumptions. The validity of the thermodynamic model was further shown by its ability, in combination with conformational and hydrodynamic models, to predict the hydrodynamic radius of the complexes over a wide range of experimental conditions.

The role and fate of antigen–antibody (Ag–Ab) complexes in the immune response depends, in part, on the size and composition of the complexes. For example, larger complexes more readily fix and activate complement (Doekes et al., 1984) and are more readily phagocytized and removed from the circulation by the reticuloendothelial system (Espinoza, 1983; Segal et al., 1983). Ag–Ab complex size and composition have been shown to directly affect single cell events such as histamine degranulation (Menon et al., 1986) as well as more complex physiological events such as those that lead to immunosuppression (Reisberg & Rossen, 1981; Caulfield et al., 1983). Additionally, size and Ab:Ag ratio affect the ability of complexes to bind to Fc receptors such as protein A (Miyama-Inaba et al., 1987). Because Ag–Ab complex size and composition are important parameters in the behavior of complexes in the immune system, a quantitative description of complex size and size distribution may prove useful.

A number of theoretical models describing size distributions of Ag–Ab complexes have been proposed (Schumaker et al., 1973, 1980; Archer & Krakauer, 1977; Steensgard et al., 1977, 1982; Moyle et al., 1983; Dembo & Goldstein, 1978; Wofsy et al., 1978; Wofsy & Goldstein, 1987), and in several cases attempts were made to fit experimental data to theory (Schumaker et al., 1973, 1980; Archer & Krakauer, 1977; Steensgard et al., 1982; Moyle et al., 1983; Husby et al., 1983; Schweitzer-Stenner et al., 1987). Although differing in detail, these models have in common the assumptions that Ag and Ab are both divalent and that equilibrium exists at all times between all possible complexes. With the exception of Steensgard et al. (1977, 1982), the models included coefficients that accounted for differences in the number of permutations of reactants yielding identical Ag–Ab complexes and the possibility that complexes may form cycles (Schumaker et al., 1973, 1980; Archer & Krakauer 1977; Moyle et al., 1983; Wofsy & Goldstein, 1987; Schweitzer-Stenner et al., 1987). Typically, the cyclization constant was assumed to vary with the number of Ab in the complex, n, as $n^{-3/2}$ (Schumaker et al., 1980; Archer & Krakauer, 1977; Moyle et al., 1983; Wofsy & Goldstein, 1987; Crothers & Metzger, 1972). Schumaker et al. (1980) included an additional term for an excess Gibbs "strain" energy of cyclization, whereas Schweitzer-Stenner et al. (1987) assumed that the cyclization constant was proportional to n^{-2}. Several researchers assumed that the association constant between Ab and Ag was invariant with complex size (Schumaker et al., 1980; Steensgard et al., 1977, 1982; Moyle et al., 1983); others allowed this to vary with n. These modifiers to the intrinsic association constant were variously called entropic parameters (Archer & Krakauer, 1977) or cross-linking constants (Wofsy & Goldstein, 1987; Schweitzer-Stenner et al., 1987). They will be referred to as polymerization constants in this study.

Experimental methods to assay complex size have included electron microscopy (Schumaker et al., 1973, 1980), light scattering (Archer & Krakauer, 1977), ultracentrifugation (Schumaker et al., 1973, 1980; Steensgard et al., 1982; Husby et al., 1983), Ag binding assays (Moyle et al., 1983), and fluorescence quenching (Schweitzer-Stenner et al., 1987). Typically, only one method has been employed in any one study. Most studies have been conducted with bivalent haptens, some of which were connected by variable-length spacers (Schumaker et al., 1973, 1980; Archer & Krakauer, 1977;

† This work was supported in part by National Institutes of Health Grants CA 45272, 01401, and 33956.

* To whom correspondence should be addressed. Present address: Department of Chemical Engineering, University of Wisconsin, Madison, WI 53706.

‡ Department of Chemical Engineering, MIT.

§ Department of Physics and Center for Materials Research, MIT.

∥ Department of Chemical and Biochemical Engineering, Rutgers University.

0006-2960/90/0429-10889$02.50/0

Schweitzer-Stenner et al., 1987), although in a few reports a protein Ag with two identical epitopes has been used (Steensgard et al., 1982; Moyle et al., 1983). Polyclonal Ab was used in some studies (Schumaker et al., 1973, 1980; Archer & Krakauer, 1977) with the implicit assumption that the affinity of the Ab population could be treated as an average apparent affinity; other researchers used monoclonal Ab (MAb) in their work (Steensgard et al., 1982; Moyle et al., 1983; Schweitzer-Stenner et al., 1987).

In work published previously, we investigated the size of Ag–Ab complexes formed upon mixing bovine serum albumin (BSA) with pairs of anti-BSA MAb. The effects of concentration, BSA:MAb molar ratio, and MAb pair on the average hydrodynamic radius of the resultant Ag–Ab complexes were demonstrated by using quasi-elastic light scattering (QLS) (Yarmush et al., 1987, 1988). We combined QLS and classical light scattering (CLS) with electron microscopy (EM) to get a detailed, quantitative picture of the average molecular weight, radius of gyration, hydrodynamic radius, size distribution, and conformation of three sets of Ag–Ab complexes at a single concentration and Ag:Ab ratio (Murphy et al., 1988).

In this report, we present additional experimental studies in which the average molecular weights of complexes prepared from the same reagents were measured by CLS over a range of concentrations and the binding of BSA to pairs of MAb at several BSA:MAb molar ratios was determined by radioimmunoassay (RIA). We describe an equilibrium model for complex formation between a pair of MAb, each with unique affinity and specificity, and an Ag containing a single epitope for each of the pair of MAb. The model in its most general form allows for cyclization and polymerization constants that are functions of the size of the complexes. The model is then simplified to include eight parameters: two intrinsic association constants, three cyclization constants, and three polymerization constants. Intrinsic association constants are determined independently. The remaining constants are simultaneously fit by using nonlinear regression to experimental data for molecular weight distribution at a single concentration (EM), average molecular weight at several concentrations (CLS), and Ag binding to each MAb pair over a range of Ag concentrations (RIA). The model, together with the fitted parameters, provides good agreement with all of the data. The thermodynamic model, in combination with conformation and hydrodynamic models, is further applied to predict hydrodynamic radius over a wide range of conditions. Finally, the values of the fitted cyclization constants are examined in comparison to predictions of a postulated theoretical model.

Materials and Methods

Bovine Serum Albumin (BSA). BSA (Pentex sulfhydryl-modified, Miles, Elkhart, IN) was dissolved in phosphate-buffered saline [PBSA: 0.15 M NaCl, 0.01 M KH_2PO_4/K_2HPO_4, and 0.02% (w/v) sodium azide, pH 7.4] and further purified by gel permeation chromatography as described previously (Murphy et al., 1988).

Monoclonal Antibodies (MAb). MAb were prepared from hybridoma cell lines designated as 5.1, 6.1, and 9.1. MAb characteristics have been reported previously (Morel et al., 1988). All MAb were subclass IgG_1. Each MAb bound noncompetitively to a different single epitope on BSA. Cells were injected intraperitoneally into pristane-primed Nu/Nu mice. Ascites fluid was tapped 10–20 days after injection, centrifuged to remove cells, and frozen at −70 °C. MAb was isolated from aliquots of thawed ascites by adsorption onto a column of CNBr-Sepharose 4B to which BSA had been covalently linked. MAb was eluted with 0.1 M glycine-HCl buffer, pH 2.5, dialyzed against PBSA, concentrated by ultrafiltration, and chromatographed on a Sephadex G-200 column to remove oligomers. Fractions corresponding to monomer IgG were collected and concentrated again by ultrafiltration. Concentration was determined by optical density measurement at 280 nm, using an extinction coefficient of 1.5 mL/(mg·cm) (Murphy et al., 1988). MAb purity was routinely checked by isoelectric focusing, sodium dodecyl sulfate–polyacrylamide gel electrophoresis, and quasi-elastic light scattering.

BSA Binding Studies. BSA was radiolabeled with ^{125}I by using the ICl method (McFarlane, 1958) or the Iodogen method (Fraker & Speck, 1978). Greater than 99% of the radioactivity was bound to protein as determined by precipitation with 10% trichloroacetic acid. Specific activity of the ^{125}I-BSA was 5.8×10^{15} counts min^{-1} mol^{-1}. Goat anti-mouse IgG Fc (Jackson Immunoresearch, Avondale, PA) was immobilized onto CNBr-Sepharose by using manufacturer's procedures. PBSA-TT [PBSA buffer with 0.05% (v/v) Tween-20 and 0.5 mg/mL porcine thyroglobulin added to reduce nonspecific adsorption to the plastic vials or to the Sepharose beads] was used as a diluent. In each assay, measured volumes of PBSA-TT and stock solutions of MAb and ^{125}I-BSA in PBSA were mixed with 50 μL of a 25% (v/v) slurry of anti-Fc beads in PBSA-TT. Volumes of diluent, MAb, and ^{125}I-BSA were chosen so that the final volume was 200 μL and the desired concentrations were achieved. The tubes were mixed with a vortex mixer and rotated end-over-end for 2–3 h at room temperature (22–24 °C). After being centrifuged for 5 min in a table-top centrifuge, 100 μL of supernatant was removed and placed in another tube; radioactivity in supernatant and precipitate tubes were counted in an Auto-Gamma 500 γ-counter (Packard Instrument, Downer's Grove, IL). Concentration of bound ^{125}I-BSA was calculated by subtracting supernatant radioactivity [counts min^{-1} (100 μL of solution)$^{-1}$] from precipitate radioactivity, and converting to concentration by dividing the difference by the specific activity. No correction was made for the volume occupied by the bead solids.

Triplicate experiments were run at each set of conditions. To measure intrinsic affinity constants, MAb was held constant at 2×10^{-8} M final concentration. ^{125}I-BSA was added to the tubes in final concentrations ranging from 2×10^{-9} to 1.2×10^{-7} M. In binding experiments with two MAb, each MAb was held constant at 1×10^{-8} M final concentration (total MAb concentration of 2×10^{-8} M). BSA concentrations ranged from 1×10^{-9} to 1.2×10^{-7} M. In these latter experiments, we assumed that the binding of MAb to anti-Fc beads did not influence the equilibrium association between MAb and BSA.

Nonspecific binding was measured in control experiments by incubating ^{125}I-BSA without MAb and measuring the concentration of bound ^{125}I-BSA as described above. ^{125}I-BSA concentrations in these experiments ranged from 1×10^{-9} to 1.2×10^{-7} M. Less than 1% of the total ^{125}I-BSA bound to the beads under these conditions; therefore, no correction for nonspecific binding was made. To measure the binding capacity of the anti-Fc beads, ^{125}I-9.1 was incubated with the beads. At an MAb concentration of 2×10^{-8} M (the concentration of MAb used in the binding experiments), >99% of the MAb was precipitated by the beads.

Light Scattering. CLS experiments were performed on a multiangle light scattering photometer described in more detail elsewhere (Murphy et al., 1988). Briefly, a vertically polarized

argon ion laser (Model 90-5, Coherent, Palo Alto, CA) operating at 488-nm wavelength was used as the light source. Scattered light from a sample was detected at 12 fixed angles (11.5–162.6°). A water bath provided temperature control and refractive index matching to the sample glass cell.

Samples were prepared by dilution of stock solutions of MAb and BSA with PBSA to the desired concentration. BSA concentrations ranged from 5×10^{-7} to 5×10^{-6} M in these samples. In all cases, concentrations of each MAb were held equal, and the Ab:BSA molar ratio was held constant at 0.9:1. Optical density of the sample at 280 nm was measured before and after light scattering to check concentration. An aliquot (8-10 mL) of solution was put into a cylindrical glass cell; the cell was sealed, and the solution was pumped continuously through a Millex GV 0.22-μm filter (Millipore, Bedford, MA) until telescopic inspection of the scattered light at a 17.4° angle showed that the sample was free of dust.

Data analysis for CLS has been described in detail previously (Murphy et al,. 1988). Briefly, light scattering from solutions of macromolecules can be represented as (Huglin, 1972)

$$\frac{Kc}{R_s(\theta)} = \frac{1}{P(q)\langle M\rangle_w} + 2Bc \tag{1}$$

where $K = 4\pi^2 n^2 (dn/dc)^2 / N_A \lambda_0^4$, n is the refractive index, dn/dc is the refractive index increment (measured to be 0.19 mL/g), c is concentration in milligrams per milliliter, λ_0 is the wavelength of light in vacuo, N_A is Avogadro's number, $R_s(\theta)$ is the measured Rayleigh ratio of the sample, $P(q)$ is a particle scattering factor, $\langle M\rangle_w$ is the weight-average molecular weight of the particles in solution, and B is the second virial coefficient. With the small particle size of our experiments, $P(q)$ can be shown to be approximated by (Sharp & Bloomfield, 1968)

$$P(q) = \left(1 + \frac{q^2\langle R_g^2\rangle_z}{3}\right)^{-1} \tag{2}$$

where $q = (4\pi n/\lambda_0) \sin(\theta/2)$ is the scattering vector, θ is the scattering angle, and $\langle R_g^2\rangle_z$ is the z-averaged mean square radius of gyration. The virial coefficient was calculated from excluded volume approximations for rods (Cassassa & Eisenberg, 1964) and for random coils (Morawetz, 1975). These calculations show that in the worst case (rods at the highest concentration and largest size in our experiments) the error in ignoring the particle interaction term ($2Bc$) is less than 4.4%. Therefore, at the low concentrations and small particle size in these experiments, eq 1 can be simplified to

$$\frac{Kc}{R_s(\theta)} = \frac{1}{\langle M\rangle_w}\left(1 + \frac{q^2\langle R_g^2\rangle_z}{3}\right) \tag{3}$$

Equation 3 was used to analyze the scattering data.

In a previous report (Yarmush et al., 1988), association and dissociation kinetics of Ag–Ab complexes were measured by QLS. Complexes that were prepared under the conditions used in the experiments reported here were shown to reequilibrate very rapidly. In most cases, association or dissociation took less than 1 min. Furthermore, no change in the size of complexes and no precipitation were detectable by QLS, even after storage at 4 °C for several months.

Electron Microscopy. Results from electron microscopy experiments were reported previously (Murphy et al., 1988). In these experiments, Ag–Ab complexes at a final BSA concentration of 8.25×10^{-7} M and a MAb_1:MAb_2:BSA molar ratio of 0.45:0.45:1 were rotary-shadowed with tungsten by means of electron-bombardment heating. The rotary-shadow technique was chosen because it exposes the sample to less harsh conditions than uranyl acetate staining. Samples were examined in a JEM 100cx electron microscope; micrographs were recorded at a magnification of 40000× and enlarged photographically to 128000×. Photomicrographs were analyzed as follows: the complexes were identified visually as open linear chains or closed cycles, individual monomers and complexes were identified, the number of units in each complex was counted, and the dimensions of each complex (contour length, end-to-end distance) were measured by using a digital image analyzer (Laboratory Computer Systems, Cambridge, MA). In previously reported experiments, we showed that electron microscopy and classical light scattering yielded consistent measurements of Ag–Ab complex size characteristics (Murphy et al., 1988).

Model Development

Thermodynamic Model. A thermodynamic model was developed that describes the equilibrium behavior of systems of two distinct, bivalent MAb (denoted Ab_1 and Ab_2), each binding to a unique site on an Ag. We assume that all species exist in reversible thermodynamic equilibrium at all times. For simple complexes composed of a single Ab and a single Ag, the equilibrium equations are

$$[Ab_1Ag] = 2K_1[Ab_1][Ag] \tag{4a}$$

$$[Ab_2Ag] = 2K_2[Ab_2][Ag] \tag{4b}$$

where K_1 and K_2 are the intrinsic association constants for the binding of monovalent Ag to a single binding site on Ab_1 and Ab_2, respectively. The statistical factor 2 is required to account for the two possible sites of association versus the single possible site for dissociation. The addition of a second Ag to the AbAg complex is described in general by the equations

$$[AgAb_1Ag] = \tfrac{1}{2}s_{1,1}K_1[Ag][Ab_1Ag] \tag{5a}$$

$$[AgAb_2Ag] = \tfrac{1}{2}s_{2,1}K_2[Ag][Ab_2Ag] \tag{5b}$$

where $s_{m,n}$ is a cooperativity factor that accounts for the effect of the presence of a bound Ag on the binding of a second Ag to an Ab, where m refers to the type of Ab (m = 1 or 2) and n is the total number of Ab in the complex. The statistical factor $^1/_2$ accounts for the single association site versus the two dissociation sites. In the development that follows, we assumed that all $s_{m,n}$ factors are equal to 1. This assumption will be justified later; minor modifications of the model equations would allow inclusion of these terms.

The binding of an Ab to an Ag that is already bound to a different Ab can be characterized in terms of the intrinsic association constant and a polymerization constant $a_{m,n}$. For the smallest such complexes, the equilibrium expressions are

$$[Ab_1AgAb_2] = 2a_{1,2}K_1[Ab_1][AgAb_2] \tag{6a}$$

$$[Ab_2AgAb_1] = 2a_{2,2}K_2[Ab_2][AgAb_1] \tag{6b}$$

Reversible thermodynamics requires that the final equilibrium concentration be independent of reaction path. Deriving the expressions for the concentration of the species Ab_1AgAb_2 from two different pathways leads to

$$\begin{aligned}[Ab_1AgAb_2] &= 2a_{1,2}K_1[Ab_1][AgAb_2] \\ &= 4a_{1,2}K_1K_2[Ab_1][Ag][Ab_2]\end{aligned} \tag{7a}$$

or

$$\begin{aligned}[Ab_1AgAb_2] &= [Ab_1Ag]2a_{2,2}K_2[Ab_2] \\ &= 4a_{2,2}K_1K_2[Ab_1][Ag][Ab_2]\end{aligned} \tag{7b}$$

Because these two expressions must be equal, it follows that $a_{1,2} = a_{2,2} = a_2$ and in general $a_{1,n} = a_{2,n} = a_n$. The set of equations can thus be simplified.

Cyclization reactions are characterized by an equilibrium constant $K_{c,m,n}$. In our system, complexes with an even number of Ab may form cycles; the equilibrium equations for the smallest cycle ($n = 2$) are

$$[Ab_1AgAb_2Ag]_{cycle} = \tfrac{1}{2}K_{c,1,2}K_1[Ab_1AgAb_2Ag] \quad (8a)$$

$$[Ab_2AgAb_1Ag]_{cycle} = \tfrac{1}{2}K_{c,2,2}K_2[Ab_2AgAb_1Ag] \quad (8b)$$

Reversible thermodynamics requires that $K_{c,1,n} = K_{c,2,n} = K_{c,n}$.

These equilibrium equations are generalized to any number of Ab (Table I). All possible species of complexes are included; there are 10 different types of linear complexes and a single type of cyclic complex. The concentration of any species can be written as a combination of the parameters K_1, K_2, a_n, and $K_{c,n}$ and the concentrations of the free species [Ag], [Ab_1], and [Ab_2]. All the equations include a term $R = 4K_1^2K_2^2[Ab_1][Ab_2][Ag]^2$. The index parameter j, which is the number of Ab in each species, can take any value from zero to infinity.

The initial concentration of the Ag and each Ab must equal the sum of the concentrations of each species multiplied by the number of Ag, Ab_1, or Ab_2 in that species. The pertinent mass balance equations are included in Table I. Strictly speaking, the mass balances are infinite sums. In practice, the equations are truncated at some value $j = j_{max}$. In our calculations, j_{max} was set equal to 20. Solutions were obtained by using a Newton–Raphson iterative technique with the total concentration of Ab and each MAb taken to be the initial value of the free concentrations. Convergence was assumed to be reached when the sum of the absolute values of the difference between the calculated mass balances and the total Ag and Ab concentrations was less than 1×10^{-20} M.

Parameter Estimation. The intrinsic association constants K_1 and K_2 were independently determined by measuring the binding of radiolabeled BSA to Ab_1 or Ab_2, respectively. The polymerization and cyclization constants were estimated from the data for each pair of MAb, which included BSA binding to two MAb (9–10 data points), $\langle M \rangle_w$ over a range of concentrations from CLS (5–10 data points), and the size distribution at a single concentration from EM (10 data points were used). Equations from Table I were used to calculate the total concentration of Ab-bound BSA, $\langle M \rangle_w$, or the size distribution of the Ag–Ab complexes at the concentrations used in the experiments as a function of the fitted parameters. To compute the molecular weight of each species, the molecular weights of the Ag and each MAb were approximated as 67 000 and 153 000, respectively.

The data were fitted to the equilibrium model with various parameter sets. The simplest cases were those where (1) $a_n = 1$ and $K_{c,n}$ was assumed to be constant for all values of n, denoted as case (1,0); (2) $K_{c,n} = 0$ and a_n was assumed to be constant for all values of n, denoted as case (0,1); and (3) a_n and $K_{c,n}$ were assumed to be constant for all values of n, denoted as case (1,1). The complexity was increased by allowing more independently determined values of a_n and $K_{c,n}$. The most complex parameter set tested included three polymerization constants, a_2, a_3, and a_n, with a_n constant for $n \geq 3$, and three cyclization constants, $K_{c,2}$, $K_{c,4}$, and $K_{c,n}$, with $K_{c,n}$ constant for $n \geq 6$.

The method of least squares was used to find the best fit of the model to the data. A Gauss–Newton algorithm was used to solve the minimization problem (Seinfeld & Lapidus, 1974).

Table I: Equilibrium and Mass Balance Equations for Thermodynamic Model

(A) Equilibrium Expressions[a]

$$[A_j] = [(AgAb_1AgAb_2)_jAg] = (\prod_{i=0}^{2j} a_i)R^j[Ag]$$

$$[B_j] = [(Ab_1AgAb_2Ag)_jAb_1] = (\prod_{i=1}^{2j+1} a_i)R^j[Ab_1]$$

$$[C_j] = [(Ab_2AgAb_1Ag)_jAb_2] = (\prod_{i=1}^{2j+1} a_i)R^j[Ab_2]$$

$$[D_j] = [(AgAb_1AgAb_2)_jAgAb_1] = 2(\prod_{i=1}^{2j+1} a_i)K_1R^j[Ag][Ab_1]$$

$$[E_j] = [(AgAb_2AgAb_1)_jAgAb_2] = 2(\prod_{i=1}^{2j+1} a_i)K_2R^j[Ag][Ab_2]$$

$$[F_j] = [(AgAb_1AgAb_2)_jAgAb_1Ag] = (\prod_{i=1}^{2j+1} a_i)K_1^2R^j[Ag]^2[Ab_1]$$

$$[G_j] = [(AgAb_2AgAb_1)_jAgAb_2Ag] = (\prod_{i=1}^{2j+1} a_i)K_2^2R^j[Ag]^2[Ab_2]$$

$$[H_j] = [(Ab_1AgAb_2Ag)_jAb_1AgAb_2] = 4(\prod_{i=1}^{2j+2} a_i)K_1K_2R^j[Ag][Ab_1][Ab_2]$$

$$[I_j] = [(AgAb_1AgAb_2)_jAgAb_1AgAb_2] = 4(\prod_{i=1}^{2j+2} a_i)K_1^2K_2R^j[Ag]^2[Ab_1][Ab_2]$$

$$[J_j] = [(AgAb_2AgAb_1)_jAgAb_2AgAb_1] = 4(\prod_{i=1}^{2j+2} a_i)K_2^2K_1R^j[Ag]^2[Ab_2][Ab_1]$$

$$[K_j] = [(AgAb_1AgAb_2)_jAgAb_1AgAb_2]_{cycle} = \frac{4}{2j+2}(\prod_{i=1}^{2j+2} a_i)K_{c,2j+2}K_1^2K_2^2R^j[Ag]^2[Ab_1][Ab_2]$$

(B) Mass Balance Equations

$$[Ag]_T = \sum_{j=0}^{j_{max}}(2j)([B_j] + [C_j]) + \sum_{j=0}^{j_{max}}(2j+1)([A_j] + [D_j] + [E_j] + [H_j]) + \sum_{j=0}^{j_{max}}(2j+2)([F_j] + [G_j] + [I_j] + [J_j] + [K_j])$$

$$[Ab_1]_T = \sum_{j=0}^{j_{max}} j([A_j] + [C_j] + [E_j] + [G_j]) + \sum_{j=0}^{j_{max}}(j+1)([B_j] + [D_j] + [F_j] + [H_j] + [I_j] + [J_j] + [K_j])$$

$$[Ab_2]_T = \sum_{j=0}^{j_{max}} j([A_j] + [B_j] + [D_j] + [F_j]) + \sum_{j=0}^{j_{max}}(j+1)([C_j] + [E_j] + [G_j] + [H_j] + [I_j] + [J_j] + [K_j])$$

[a] $R = 4K_1^2K_2^2[Ab_1][Ab_2][Ag]^2$. Polymerization constants a_0 and $a_1 = 1$.

Results

Experimental Data. (A) Determination of Intrinsic Association Constants. Data for binding of ^{125}I-BSA to individual MAb are plotted in the form of adsorption isotherms in Figure 1A. The data were fit by nonlinear least-squares regression to the Langmuir adsorption equation:

$$[Ag]_B = \frac{bK_a[Ab]_T[Ag]_F}{1 + K_a[Ag]_F} \quad (9)$$

where K_a is the intrinsic association constant (in liters per mole), b is the number of binding sites ($b = 2$ for bivalent

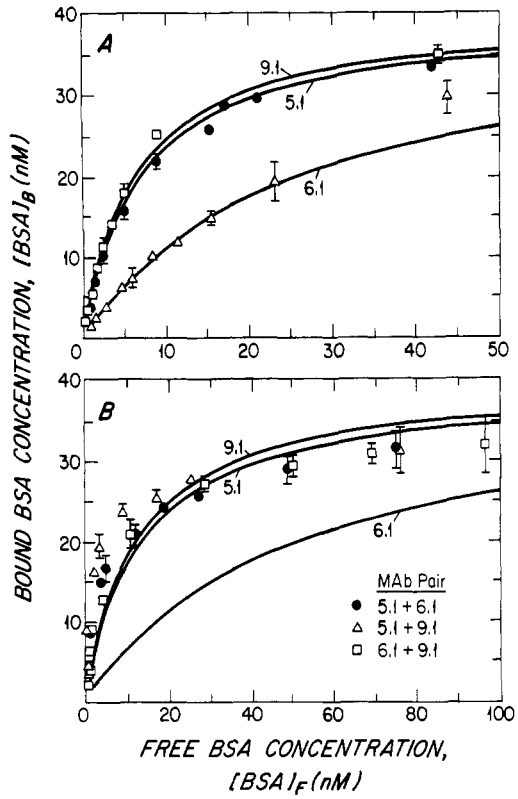

FIGURE 1: Adsorption isotherms for binding of ^{125}I-BSA to (A) individual MAb, with $[Ab]_T = 2 \times 10^{-8}$ M in each case, or (B) pairs of MAb, with $[Ab_1]_T = [Ab_2]_T = 1 \times 10^{-8}$ M. Data points represent mean ± SD of triplicate samples. Solid lines in both (A) and (B) are least-squares fits of the data for individual MAb.

Table II: *Ka* and *b* for MAb Binding to BSA

	adsorption isotherm[a]		Scatchard plot[b]	
MAb	K_a ($M^{-1} \times 10^{-7}$)	*b*	K_a ($M^{-1} \times 10^{-7}$)	*b*
5.1	14 ± 1	2.0 ± 0.1	14 ± 1	2.0 ± 0.1
6.1	3.8 ± 0.3	2.0 ± 0.1	3.4 ± 0.4	2.2 ± 0.1
9.1	16 ± 1	2.0 ± 0.1	15 ± 1	2.0 ± 0.1

[a] Fit obtained by using eq 9. [b] Fit obtained by using eq 10.

antibody), $[Ab]_T$ is the total concentration of Ab, and $[Ag]_B$ and $[Ag]_F$ are the concentration of bound and free Ag, respectively. The same data were fit by linear least-squares regression to the Scatchard equation:

$$[Ag]_B/[Ag]_F = bK_A[Ab]_T - K_a[Ag]_B \qquad (10)$$

Values of K_a and *b* fitted by using both equations are included in Table II. The values of K_a for 5.1 and 9.1 are slightly lower than those measured in a previous study (Murphy et al., 1988). The data for each MAb fit a straight line ($r = 0.99$, 0.95, and 0.99 for 5.1, 6.1, and 9.1, respectively), thereby justifying the assumption that $s_{1,1} = s_{2,1} = 1$ in the application of the model to our system. In all subsequent calculations with the thermodynamic model, the values of K_a from the fit to eq 9 were used for K_1 and K_2.

(B) BSA Binding to MAb Pairs. Binding of ^{125}I-BSA to pairs of MAb is plotted as adsorption isotherms in Figure 1B. The results of the fit to eq 9 for the three individual MAb from Figure 1A are also plotted for comparison. Scatchard plots of the data (not shown) show steeper initial slopes for pairs of MAb than for individual MAb, indicative of higher average apparent affinity constants for the MAb pairs, particularly for 5.1 + 9.1. The lower asymptotic values of bound BSA for MAb pairs (Figure 1B) than for single MAb (Figure 1A) are

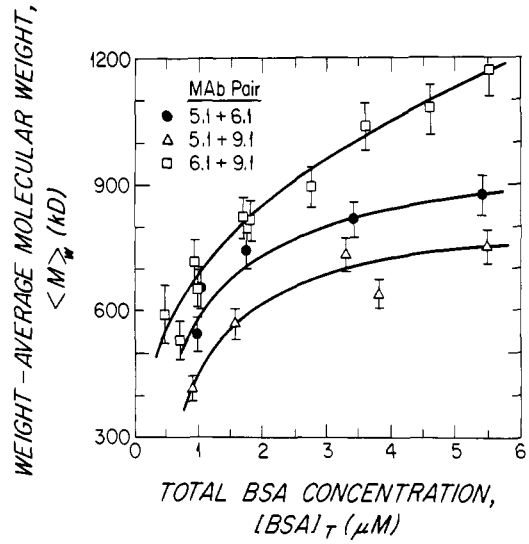

FIGURE 2: $\langle M \rangle_w$ as a function of concentration for three sets of Ag–Ab complexes from light scattering experiments. In all cases, $[Ab_1]_T = [Ab_2]_T$, and $[Ab]_T/[Ag] = 0.9$. Standard deviations were calculated by propagation of error analysis, using the standard deviation of the intensity measurements at zero angle and assuming an error in concentration of ±15% and in dn/dc of ±0.005 mL/g. Solid lines were drawn by eye.

due to the presence of cycles and/or complexes containing two or more Ab. In constrast to the Scatchard plots for individual MAb, MAb pairs show significant deviations from linearity.

(C) Light Scattering. $\langle M \rangle_w$ of complexes of 5.1 + 6.1, 5.1 + 9.1, and 6.1 + 9.1 were measured by CLS as a function of BSA concentration, keeping the Ag:Ab molar ratio constant and equal to 0.9:1 (Figure 2). The average size of the complexes increased with increasing concentration; however, there was variation in the behavior of the three pairs studied. Complex size increased in the order 5.1 + 9.1 < 5.1 + 6.1 < 6.1 + 9.1, a pattern consistent with that reported previously for measurements of $\langle R_h \rangle_z$ (Yarmush et al., 1988).

Data Analysis. Parameter Estimation. The data for BSA binding to pairs of MAb, $\langle M \rangle_w$ from CLS, and complex size distribution from EM (Murphy et al., 1988) were used to determine cyclization and polymerization constants in the equilibrium model. The constants evaluated by fitting to three cyclization and three polymerization constants are tabulated in Table III, along with values of the change in Gibbs free energy, defined by

$$\Delta G = -RT \ln K \qquad (11)$$

where R is the ideal gas constant, T is the absolute temperature (293 K), and K represents K_a, $K_{c,n}$, or a_n. $K_{c,2}$ was smallest for 5.1 + 6.1 and largest for 5.1 + 9.1. For 5.1 + 6.1 and 6.1 + 9.1, $K_{c,n}$ increased with increasing n, whereas for 5.1 + 9.1, the opposite was true. The large standard deviation in the fitted cyclization constants reflects the fact that the data are sensitive only to the order of magnitude of $K_{c,n}$. The polymerization constants ranged from 0.05 to 0.25. Values of a_2 were very similar regardless of the MAb pair; the same was true for a_3. For 5.1 + 6.1 and 6.1 + 9.1, a_n was very similar to a_2, whereas for 5.1 + 9.1, a_n was half a_2. For all three MAb pairs, a_3 was greater than a_2. Correlation coefficients were generally low, except for those of a_2 and a_n for all three MAb pairs and those of $K_{c,n}$ and a_n for 5.1 + 6.1 and 5.1 + 9.1 (Murphy, 1989).

Parameter fits to subsets of the data were performed (Murphy, 1989). When only EM and CLS data were evaluated, the fitted parameters were virtually identical with those obtained from a fit to all the data (base case), reflecting an

Table III: Fitted Equilibrium Parameters and Gibbs Free Energy Changes

MAb	association constant, K_a ($M^{-1} \times 10^{-7}$)	Gibbs free energy change, ΔG_a (kcal/mol)
5.1	14 ± 1	−10.9
6.1	3.8 ± 0.3	−10.2
9.1	16 ± 1	−11.0

Ab–Ab complex	cyclization constant ($M \times 10^8$)			Gibbs free energy change (kcal/mol)		
	$K_{c,2}$	$K_{c,4}$	$K_{c,n}$	$\Delta G_{c,2}$	$\Delta G_{c,4}$	$\Delta G_{c,n}$
5.1 + 6.1	0.65 ± 0.69	1.5 ± 1.8	6.9 ± 18	11.0	10.5	9.6
5.1 + 9.1	7.5 ± 1.2	5.5 ± 2.2	0.53 ± 10	9.6	9.7	11.1
6.1 + 9.1	1.5 ± 0.6	7.8 ± 2.8	8.6 ± 7.5	10.5	9.5	9.5

Ab–Ag complex	polymerization constant			Gibbs free energy change (kcal/mol)		
	a_2	a_3	a_n	$\Delta G_{a,2}$	$\Delta G_{a,3}$	$\Delta G_{a,n}$
5.1 + 6.1	0.13 ± 0.04	0.22 ± 0.07	0.10 ± 0.02	1.2	0.9	1.3
5.1 + 9.1	0.11 ± 0.02	0.17 ± 0.04	0.05 ± 0.01	1.3	1.0	1.7
6.1 + 9.1	0.13 ± 0.03	0.25 ± 0.06	0.16 ± 0.01	1.2	0.8	1.1

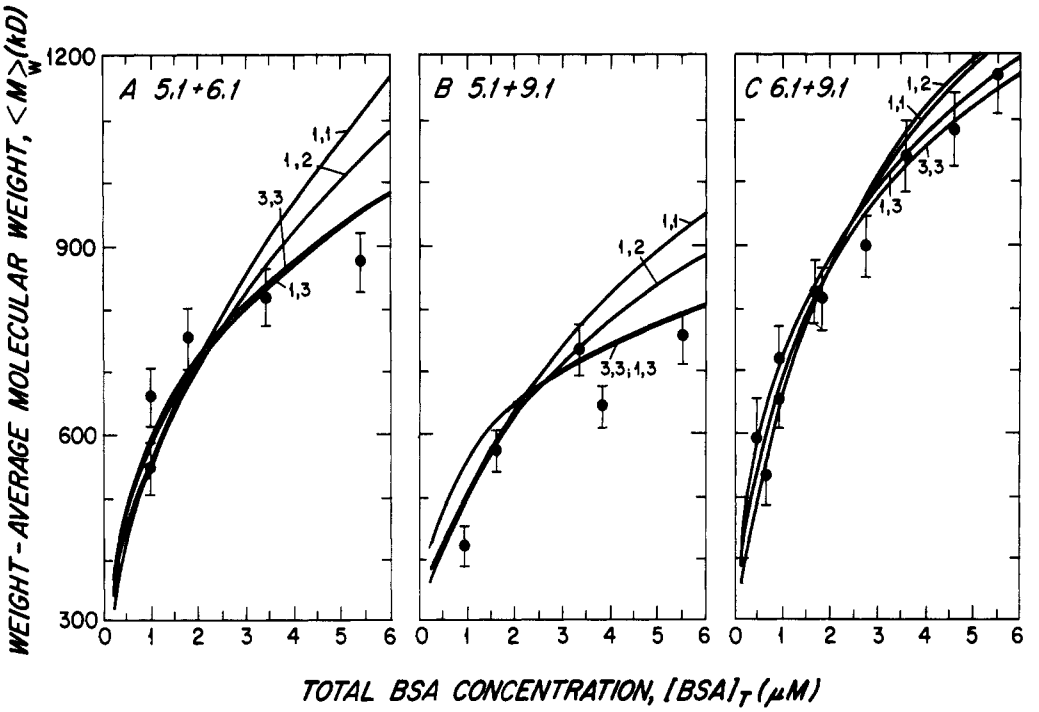

FIGURE 3: Effect of the number of fitted polymerization constants or cyclization constants on the fit of the model to $\langle M \rangle_w$. The data points are from Figure 2. The fitted values are shown by solid lines. The fitted parameters were determined by nonlinear regression as described in the text. Numbers associated with each curve refer, in order, to the number of fitted cyclization constants and the number of fitted polymerization constants. For example, 1,2 refers to the case where $K_{c,2} = K_{c,4} = K_{c,n}$ and $a_2 \neq a_3 = a_n$. (A) 5.1 + 6.1; (B) 5.1 + 9.1; (C) 6.1 + 9.1.

insensitivity to the RIA data. With EM data alone, the only significant difference occurred in a_n, which was uniformly higher than for the base case. With CLS data alone, convergence was not obtained for 5.1 + 6.1. In the other two cases, the best-fit parameters were higher for $K_{c,n}$ and similar for a_n in comparison to the base case; the uncertainty in both parameters increased substantially. Parameters obtained by fitting RIA data alone were very different than any of the other cases, with a much lower $K_{c,n}$ and a much higher a_n. Uncertainties in both parameters were very high.

Analysis of the same data were carried out with parameter sets having fewer constants (Murphy, 1989). Predictions of the equilibrium model with selected parameter sets are compared to experimental data in Figures 3–6. Adding polymerization constants markedly improved the fit to $\langle M \rangle_w$ data for 5.1 + 6.1 and 5.1 + 9.1 (Figure 3), especially at the higher concentrations. Changing the number of cyclization constants had little or no effect. Adding polymerization and/or cyclization constants improved the agreement for 6.1 + 9.1, but the effects were smaller than for either of the other MAb pairs.

Reducing the number of polymerization constants had a large effect on the ability to predict the size distribution of linear complexes from EM data for 5.1 + 9.1 (Figure 4), progressively less effect for 5.1 + 6.1 and 6.1 + 9.1, and relatively little effect on the distribution of cyclic complexes (Figure 5). Changing the number of cyclization constants had virtually no effect on the predicted size distribution of linear complexes but had a comparatively large effect on the agreement with data for the size distribution of cyclic complexes (Figure 5), especially for 5.1 + 6.1 and 6.1 + 9.1 when only one value of $K_{c,n}$ for all n was used to fit the data. BSA binding data were insensitive to the number of parameter values (Figure 6), largely because the experiments were conducted at low concentrations, where the larger complexes that influence higher order parameters were not present.

Conformation-Dependent Properties. (A) Hydrodynamic Radius. In previous experiments (Yarmush et al., 1988), $\langle R_h \rangle_z$ of 5.1 + 6.1, 5.1 + 9.1, and 6.1 + 9.1 was measured by QLS at several concentrations and Ag:Ab molar ratios. In order to compare this data with theoretical prediction, we made

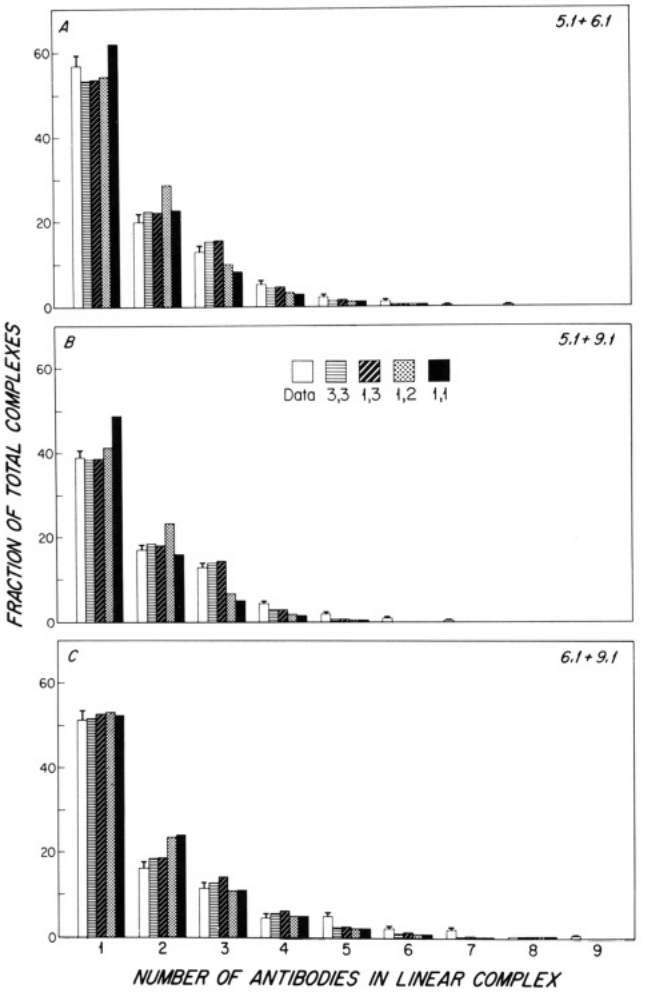

FIGURE 4: Effect of the number of fitted polymerization constants on the fit of the model to the distribution of linear complexes as estimated by EM. The data are from Figure 5 in Murphy et al. (1988). Numbers associated with each bar refer, in order, to the number of fitted cyclization constants and the number of fitted polymerization constants. (A) 5.1 + 6.1; (B) 5.1 + 9.1; (C) 6.1 + 9.1.

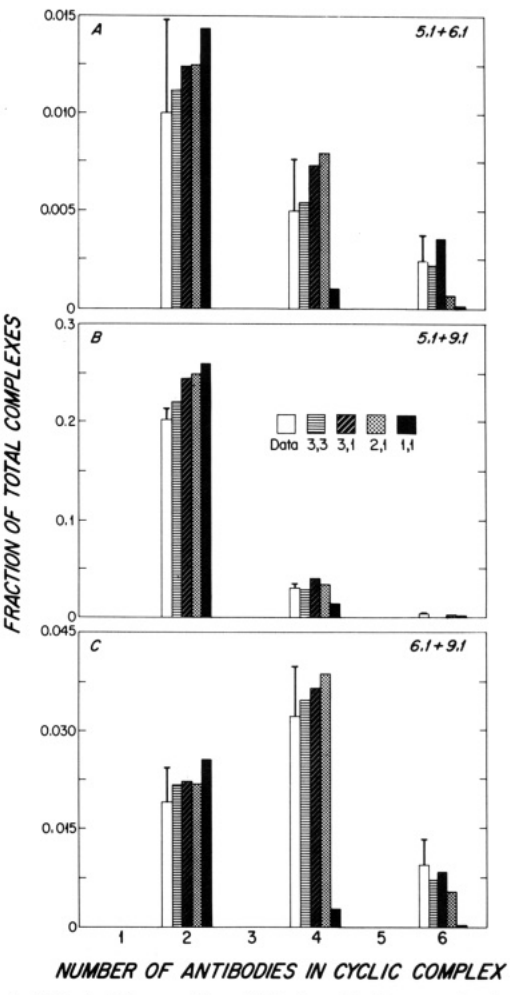

FIGURE 5: Effect of the number of fitted cyclization constants on the fit of the model to the distribution of cyclic complexes as estimated by EM. The data are from Figure 5 in Murphy et al. (1988). Numbers associated with each bar refer, in order, to the number of fitted cyclization constants and the number of fitted polymerization constants. (A) 5.1 + 6.1; (B) 5.1 + 9.1; (C) 6.1 + 9.1. Note that the vertical scales are different in the three panels.

use of Porod–Kratky theory, which we previously employed (Murphy et al., 1988) to describe the complexes as semiflexible wormlike chains. In our prior study, we estimated conformation parameters by fitting experimental data to predictions of conformational and hydrodynamic models (Yamakawa & Fujii, 1973; Fujii & Yamakawa, 1975). This same theory was applied to the measurements made in this study. Briefly, the species distribution at several combinations of concentrations and molar ratios were calculated from the thermodynamic model and the parameters in Table III. Then, by using the contour length L_i evaluated from electron microscopy data and the persistence length a and chain diameter d previously estimated (Murphy et al., 1988), the hydrodynamic radius R_{hi} for each complex size was estimated from Porod–Kratky theory (Yamakawa & Fujii, 1973; Fujii & Yamakawa, 1975). $\langle R_h \rangle_z$ was calculated from

$$\langle R_h \rangle_z = \left(\frac{\sum N_i M_i^2 (R_h)_i^{-1}}{\sum N_i M_i^2} \right)^{-1} \quad (12)$$

where N_i and M_i are the number fraction and molecular weight, respectively, of complex i, which were calculated from the equilibrium model. The predicted values are compared with the QLS data in Figures 7 and 8. Agreement between prediction and data is generally satisfactory. The fit is poorest in antigen excess (Figure 8); the reason for this is unknown.

(B) Theoretical Estimate of Cyclization Parameters. Attempts were made to estimate cyclization constants from theoretical considerations. We postulated that the cyclization constants $K_{c,n}$ were composed of two terms, a configurational term $K_{f,n}$ and a steric term a_n:

$$K_{c,n} = a_n K_{f,n} \quad (13)$$

Furthermore, $K_{f,n}$ was assumed to be equal to the number density (on a molar basis) of configurations allowed when the distance between the two ends of the chain is zero. To calculate this number density, the density distribution function $f(r,s)$ for r, where r is the distance between two points on a Porod–Kratky chain separated by a contour length s, was used (Schmidt & Stockmayer, 1984; Koyama, 1973):

$$f(r,s) = \frac{1}{2\pi^{1/2}AB} \frac{1}{4\pi r} \left\{ \exp\left(\frac{-(r-B)^2}{2A} \right) - \exp\left(\frac{-(r+B)^2}{2A} \right) \right\} \quad (14)$$

where A and B are constants related to mean end-to-end distances $\langle R^2 \rangle$ and $\langle R^4 \rangle$ of the chain. $\langle R^2 \rangle$ and $\langle R^4 \rangle$ were calculated for several choices of persistence length and contour length from equations in Koyama (1973). $f(r,s)$ was then calculated from eq 14 for the case where s is the contour length of the entire chain and r approaches zero. The results were

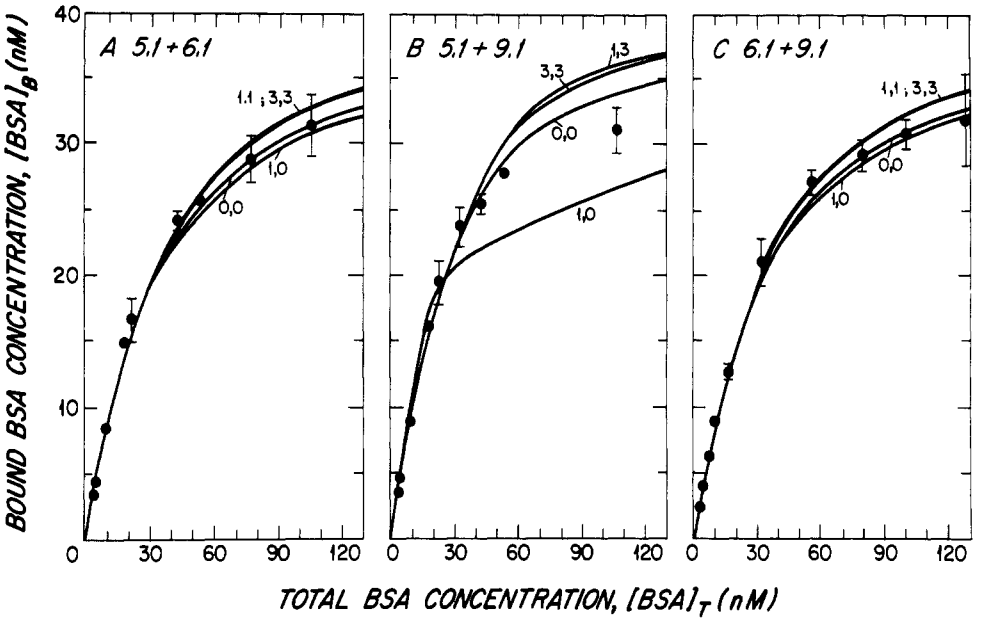

FIGURE 6: Effect of various fitted parameter sets on the fit of the model to BSA binding data. The data points are from Figure 2. The fitted values are connected by solid lines. Numbers associated with each curve refer, in order, to the number of fitted cyclization constants and the number of fitted polymerization constants. The curve 0,0 denotes the case where $a_2 = a_3 = a_n = 1$ and $K_{c,2} = K_{c,4} = K_{c,n} = 0$. (A) 5.1 + 6.1; (B) 5.1 + 9.1; (C) 6.1 + 9.1.

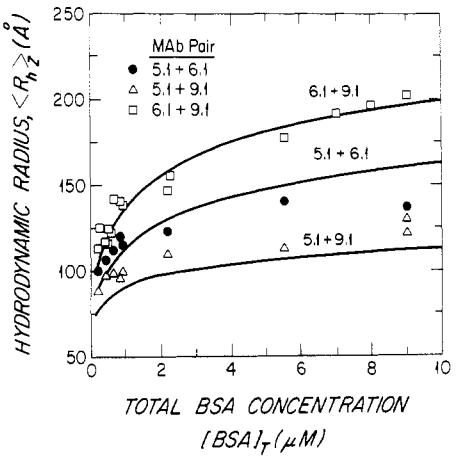

FIGURE 7: Effect of Ag concentration on $\langle R_h \rangle_z$ from QLS measurements (circles) reported in Figure 1 of Yarmush et al. (1988). Predicted values (solid lines) were calculated as described in the text, using Porod–Kratky parameters a = 430, 91, and 205 Å and d = 83, 85, and 110 Å for 5.1 + 6.1, 5.1 + 9.1, and 6.1 + 9.1, respectively (Murphy et al., 1988). In all cases, $[Ab_1]_T = [Ab_2]_T$, and $[Ab_1]_T$:$[Ag]_T$ = 0.45.

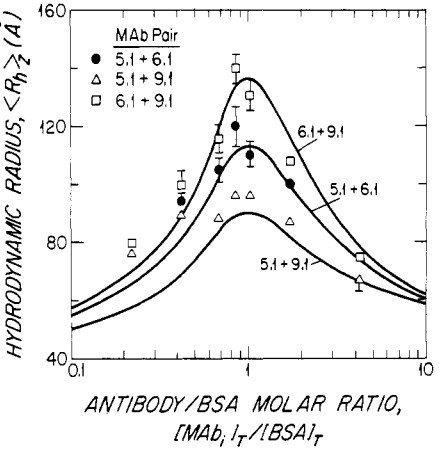

FIGURE 8: Effect of Ag:Ab ratio on $\langle R_h \rangle_z$ from QLS measurements (circles) reported in Figure 3 of Yarmush et al. (1988). Predicted values (solid lines) were calculated as described in the text with the Porod–Kratky parameters listed in the caption to Figure 8. In all cases, $[Ab_1]_T = [Ab_2]_T$, and concentrations followed the relation $[Ab_1]_T + [Ab_2]_T + [Ag]_T = 1.5 \times 10^{-6}$ M.

converted to molar units by dividing by Avogadro's number. The theory predicts that $K_{f,n}$ decreases rapidly as the persistence length increases and the chain becomes more rodlike. $K_{f,n}$ increases with increasing n at large values of persistence length, whereas at low persistence lengths, where the wormlike chain approaches a random coil configuration, $K_{f,n}$ decreases with increasing n.

The cyclization constants $K_{c,n}$ evaluated by fitting of the data were divided by the corresponding fitted value of a_n (Table III) to estimate $K_{f,n}$ and compared to the theoretical values calculated as a function of the average persistence lengths of the complexes (430 Å for 5.1 + 6.1, 91 Å for 5.1 + 9.1, and 205 Å for 6.1 + 9.1). For 5.1 + 6.1, $K_{f,n}$ calculated from the data were generally greater than predicted by eq 14. $K_{f,n}$ increased substantially with increasing n, as predicted by the theory in this persistence length range. For 5.1 + 9.1, the experimentally determined values of $K_{f,n}$ were lower than predicted but within the error of the persistence length. At the persistence length estimated for 5.1 + 9.1, the theory predicted that $K_{f,2} < K_{f,6} < K_{f,4}$; the fitted configurational constants followed this pattern. With 6.1 + 9.1, $K_{f,n}$ was slightly greater than predicted. In this persistence length region, the theory predicted that $K_{f,2} < K_{f,4} < K_{f,6}$. The fitted parameters followed the pattern $K_{f,2} < K_{f,4} = K_{f,6}$.

Discussion

In previous studies (Yarmush et al., 1988; Murphy et al., 1988), we characterized the size properties of Ag–Ab complexes made from three pairs of MAb, using CLS, QLS, and EM. The complexes exhibited very different molecular weight distributions, which were not simply related to the intrinsic association constants of the individual MAb comprising the pair, as well as differences in the incidence of cyclic complexes. The size of the complexes increased in the order 5.1 + 9.1 < 5.1 + 6.1 < 6.1 + 9.1. The pair 5.1 + 9.1 formed many more small cyclic complexes than the other two pairs. In this work,

we investigated the behavior of these complexes under a wider range of concentrations, developed a thermodynamic model to describe the equilibrium size distribution, and calculated thermodynamic parameters for the three MAb pairs. By using three polymerization and three cyclization constants, we were able to achieve a good fit of the thermodynamic model to the combined CLS, EM, and RIA data. The validity of the thermodynamic model was further shown by its ability, in combination with conformational and hydrodynamic models, to predict $\langle R_h \rangle_z$ for the Ag–Ab complexes over a range of concentrations and Ag–Ab molar ratios. An alternative method to validate the model would have been to obtain CLS data at several Ag–Ab ratios; these experiments have not been done, partially because of the large amount of MAb required for CLS experiments compared to QLS experiments.

This work differs from previously published studies in several respects: well-characterized MAb with independently measured association constants were used, three complementary experimental techniques were exploited to get a quantitative description of the complexes, a protein Ag rather than a hapten was used, and three different pairs of MAb that produce three different kinds of complexes were employed.

Comparison of Results with Other Studies. The size distribution of Ag–Ab complexes has been studied previously; theoretical thermodynamic models have been proposed to predict size distributions. Many of these investigators employed polyclonal Ab (Schumaker et al., 1973, 1980; Archer & Krakauer, 1977; Husby et al., 1983), which are inherently heterogeneous in association constants, and divalent haptens (Schumaker et al., 1973, 1980; Archer & Krakauer, 1977; Schweitzer-Stenner et al., 1987). Exceptions were Steensgard et al. (1982) and Moyle et al. (1983), both of whom used MAb and protein Ag. However, the intrinsic association constant was not independently measured in the former case. In the latter case, technical difficulties, including the probable presence of a significant quantity of myeloma protein contamination, led to concerns about the quantitative validity of the results.

Previous workers typically used only a single type of experimental data. In some cases, ultracentrifugation was used to obtain an estimate of the size distribution (Schumaker et al., 1973; Steensgard et al., 1982), but no account was taken of the possible dissociation of complexes during ultracentrifugation due to dilution (Yarmush et al., 1987). Archer and Krakauer (1977) used classical light scattering to measure the change in molecular weight of Ag–Ab complexes with increasing concentration of monovalent hapten. This experimental technique is an improvement on ultracentrifugation since the possibility of dissociation due to dilution is eliminated; however, individual complexes cannot be resolved. Prior to our work, size distributions from electron microscopy have been used only qualitatively (Schumaker et al., 1973, 1980). Ag binding assays (Moyle et al., 1983) and fluorescence quenching titration (Schweitzer-Stenner et al., 1987) have been used; these techniques measure the number of occupied Ab binding sites and are not a direct measurement of the size or conformation of the complexes.

Our fitted values for cyclization and polymerization constants were compared to those reported in other studies. Differences between our values and those from other studies probably resulted from differences in size and/or flexibility of the Ag and Ab and/or from the experimental methods used to determine the parameters. Schumaker et al. (1973) estimated a strain of 5 kcal/mol for the formation of a closed Ab_2Ag_2 cycle and 2.5 kcal/mol for the case where a bivalent hapten (α,ϵ-di-DNP-lysine) is bound to two bivalent Ab. These values can be converted by use of eq 11 to a cyclization constant of 1.9×10^{-4} M and a polymerization constant of 0.014. Archer and Krakauer (1977) estimated cyclization constants of 1×10^{-5} to 7×10^{-4} M and polymerization constants of 0.12–0.41 for the case where the Ag was a random coil polymer to which a hapten (DNP) was added at each end and the Ab was either equine IgG or IgG(T). Their values are not directly comparable to ours because their polymerization constants were applied to binding of either Ag or Ab to a complex. Moyle et al. (1983) estimated a cyclization constant of 3×10^{-4} M for their complexes of MAb and human chorionic gonadotropin. No polymerization constants were included in their model. In their work on Ag–Ab complex formation from mouse IgE Ab and a series of divalent DNP haptens linked by spacers of different length and flexibility, Schweitzer-Stenner et al. (1987) estimated cyclization constants of 1×10^{-3} to 1.4×10^{-6} M and polymerization constants equivalent to 0.03–0.38. This comparison suggests that cyclization occurs less readily with protein Ag than with flexible divalent hapten.

Theoretical Basis for Cyclization and Polymerization Constants. Attempts to calculate cyclization constants from density distributions of Porod–Kratky chains were only partially successful. However, given the uncertainty of the estimated persistence lengths and the qualitative agreement between theoretically predicted and experimentally determined configurational constants, it is reasonable to attribute the magnitude of the cyclization constants primarily to configurational losses. Complexes with larger persistence lengths should theoretically have lower cyclization constants because of their greater stiffness; this is indeed what we saw. The stiffness of the chain makes it more difficult to form complexes when the chain is short. On the other hand, as the chain gets longer, the chain ends are less likely to find each other. The relative importance of these two opposing effects depends on the contour length, which is a function of the number of Ab in the complex, and the persistence length, which appears to be an inherent function of the geometry and the flexibility of the Ag–Ab bond.

Configurational constants generally increased with increasing number of Ab. This pattern is in contrast to other studies, where it was assumed that cyclization followed random-walk statistics, and thus cyclization constants decreased with increasing n. Schumaker et al. (1980) calculated an excess ΔG associated with strain energy in cycle formation. As the authors pointed out, however, this estimated excess Gibbs free energy may result simply from the inexactness of the mathematical description of freely jointed chains at low values of n, since the application of this theory to small n is inappropriate (Flory, 1953). This strain energy may be more appropriately accounted for by use of a more realistic model of complex conformation than the random coil. The higher cyclization constants obtained when the Ag is a divalent hapten connected by a flexible spacer (Archer & Krakauer, 1977; Schweitzer-Stenner et al., 1987) may result from the greater flexibility of these complexes, in which case the assumption of random-walk statistics may be appropriate.

The polymerization constants account for a small loss (about 1 kcal/mol) in Gibbs free energy of association; however, this loss makes a large difference in the resulting size of the complexes. The cause of the loss in Gibbs free energy is uncertain. Possible contributions include loss of translational and rotational Gibbs free energy upon association of a single Ab and Ag as compared to that of a complex and single Ab (Janin

& Chothia, 1978), steric restriction arising from crowding of two Ab binding to the same Ag, or burial of unoccupied Ag or Ab binding sites due to coiling of the complex. Archer and Krakauer (1977) attributed their polymerization constants to losses of configuration of the random coil Ag when one end is anchored by an Ab. Schumaker et al. (1973) attributed their observations to burial of one end of the hapten deep within the Ab binding pocket, thereby preventing complete association at all points at the other binding site. The importance of this mechanism probably depends on the Ag size and the relative distance between the two epitopes. One might anticipate that burial of the binding site is a factor only in systems with smaller Ag than ours.

Significance of Fitted Parameters. Achieving a good fit of the model to the data required three cyclization and three polymerization constants. Attempts were made to fit the data to fewer parameters; in fact, in our initial work we tried fitting the data to a single cyclization constant. All six parameters could not be justified statistically (Murphy, 1989). However, no single, smaller set of parameters was equally good at fitting the data for all three MAb pairs. Additional polymerization constants significantly improved the fit for 5.1 + 6.1 and 5.1 + 9.1, whereas additional cyclization constants significantly improved the fit for 6.1 + 9.1. The total number of fitted parameters could be reduced to two (one cyclization constant and one polymerization constant) if generally valid correlations for the effect of n on these constants were available.

Usefulness of Various Experimental Techniques. Attempts were made to evaluate the thermodynamic parameters by fitting to only one or two types of experimental data rather than all three sets. With either the EM data alone or the CLS plus EM data together, the regression easily converged; the resulting parameters were similar to the results from the fit to all three data sets. With CLS data alone, uncertainties in the fitted parameters were substantially higher than for the composite data set, and correlation coefficients were negative and large. This reflects the opposing effects that cyclization and polymerization constants have on average molecular weights and the lack of sensitivity of a measurement of average molecular weight to details about the size distribution. In fact, several similarly good fits to CLS data alone can be obtained by nonunique sets of parameter values (data not shown). Inclusion of size distributions from EM data in the analysis serves to pin down the values of the cyclization parameters, allowing unique values for the polymerization constants to be determined.

BSA binding data alone was unsuccessful in determining parameter values. Since only small complexes formed at the concentrations used in RIA experiments, the results were insensitive to parameters applicable where $n > 2$. Furthermore, increasing a_n had similar effects on the shape of the isotherm as did increasing $K_{c,n}$; the two parameters were positively correlated with respect to the RIA data. Finally, Ag–Ab interactions may have been affected by the binding of Ab to immobilized anti-Fc.

Thus, the combination of EM and CLS data was important for successful estimation of thermodynamic parameters. EM data were tedious to obtain and could have been subject to artifacts. Coupling EM data with solution measurements of $\langle M \rangle_w$ ensured that the micrographs represented the solution behavior of the complexes as well. Furthermore, CLS data were more readily obtained over a range of concentrations and molar ratios than EM data and therefore contributed significant supportive information.

Concluding Remarks. Our work suggests that small changes in cyclization or polymerization constants have a profound effect on the ability of Ab to combine with Ag and form large complexes. The ability to form cycles or add to the chain may be strongly dependent on the size of the Ag and the relative location of the epitopes. The flexibility of the complexes, as measured by the persistence length, is an important determinant of the magnitude of the cyclization constants. The inability of certain orientations to form large complexes reduces the ability of the immune system to clear the Ag and hence leads to persistence of the complex in the circulation.

Recently, the crystal structure of human serum albumin (HSA) at 6-Å resolution was reported (Carter et al., 1989). Because the primary sequence of BSA is highly homologous with HSA, we anticipate that the tertiary structure of BSA is similar to HSA. This recent report motivates a closer look at the specific amino acids on BSA that form the antigenic sites for the MAb we employed. Models could then be constructed that would be consistent with the molecular details of Ag–Ab binding as well as with the macroscopic data we obtained. Such models would help to elucidate the topological factors that influence the overall size and conformation of Ag–Ab complexes.

ACKNOWLEDGMENTS

This work was supported in part by National Institutes of Health Grants CA 45272, 01401, and 33956. R.M.M. was a Whitaker Health Sciences Fund Fellow. M.L.Y. is a Lucille P. Markey Scholar in Biomedical Science. We gratefully acknowledge Prof. George Benedek for use of light-scattering facilities in his laboratory.

REFERENCES

Archer, B. G., & Krakauer, H. (1977) *Biochemistry 16*, 618–627.

Carter, D. C., He, X.-M., Munson, S. H., Twigg, P. D., Gernert, K. M., Broom, M. B., & Miller, T. Y. (1989) *Science 244*, 1195–1198.

Cassassa, D. F., & Eisenberg, H. (1964) *Adv. Protein Chem. 19*, 287–395.

Caulfield, M. J., Luce, K. J., Proffitt, M. R., & Cery, H. (1983) *J. Exp. Med. 157*, 1713–1725.

Crothers, D. M., & Metzger, H. (1972) *Immunochemistry 9*, 341–357.

Dembo, M., & Goldstein, B. (1978) *J. Immunol. 121*, 345–353.

Espinoza, L. R. (1983) in *Circulating Immune Complexes: Their Clinical Significance* (Espinoza, L. R., & Osterland, C. K., Eds.) Futura Publishing Co., Mount Kisco, NY.

Flory, P. J. (1953) *Principles of Polymer Chemistry*, Cornell University Press, Ithaca, NY.

Fraker, P. J., & Speck, J. C. (1978) *Biochem. Biophys. Res. Commun. 80*, 849–857.

Fujii, M., & Yamakawa, H. (1975) *Macromolecules 8*, 792–799.

Huglin, M. N. (1972) *Light Scattering from Polymer Solutions*, pp 165–331, Academic Press, New York.

Husby, S., Steensgard, J., Feldt-Rasmussen, V., & Date, J. (1983) *Immunology 48*, 401–409.

Janin, J., & Chothia, C. (1978) Role of hydrophobicity in the binding of coenzymes. *Biochemistry 17*, 2943–2948.

Koyama, R. (1973) *J. Phys. Soc. Jpn. 34*, 1029–1038.

McFarlane, A. S. (1958) *Nature 182*, 53–54.

Menon, A. K., Holowka, K., Webb, W. W., & Baird, B. (1986) *J. Cell. Biol. 102*, 541–550.

Miyama-Inaba, M., Ohno, T., Inaba, K., Ajisaka, K., Suzuki, R., Kumagai, K., & Masuda, T. (1987) *Immunology 61*, 43–50.
Morawetz, H. (1975) *Macromolecules in Solution*, pp 189–192, Wiley and Sons, Inc., New York.
Morel, G. A., Yarmush, D. M., Colton, C. K., Benjamin, D. C., & Yarmush, M. L. (1988) *Mol. Immunol. 25*, 7–16.
Moyle, W. R., Lin, C., Corson, R. L., & Ehrlich, P. H. (1983) *Mol. Immunol. 20*, 439–482.
Murphy, R. M. (1989) Antigen–Antibody Complexes: Size, Structure and Reactivity with Protein A. Ph.D. Thesis, Massachusetts Institute of Technology, Cambridge, MA.
Murphy, R. M., Slayter, H., Schurtenberger, P., Chamberlin, R. A., Colton, C. K., & Yarmush, M. L. (1988) *Biophys. J. 54*, 45–56.
Reisberg, M. A., & Rossen, R. D. (1981) *Clin. Exp. Immunol. 46*, 443–452.
Schmidt, M., & Stockmayer, W. H. (1984) *Macromolecules 17*, 509–514.
Schumaker, B. N., Green, G., & Wilder, R. L. (1973) *Immunochemistry 10*, 521–528.
Schumaker, V. N., Seegan, G. W., Smith, C. A., Ma, S. K., Rodwell, J. D., & Schumaker, M. F. (1980) *Mol. Immunol. 17*, 413–423.
Schweitzer-Stenner, R., Licht, A., Luscher, I., & Pecht, I. (1987) *Biochemistry 26*, 3602–3612.
Segal, D. N., Dower, S. K., & Titus, J. A. (1983) *J. Immunol. 130*, 130–137.
Seinfeld, J. H., & Lapidus, L. (1974) *Mathematical Methods in Chemical Engineering. Vol. 3. Process Modeling, Estimation and Identification*, Prentice-Hall, Englewood Cliffs, NJ.
Sharp, P., & Bloomfield, V. A. (1968) *Biopolymers 6*, 1201–1211.
Steensgard, J., Liu, B. M., Cline, G. B., & Moller, N. P. H. (1977) *Immunology 32*, 445–456.
Steensgard, J., Jacobson, C., Lowe, J., Ling, N. R., & Jefferis, R. (1982) *Immunology 46*, 751–760.
Wofsy, C., & Goldstein, B. (1987) *Mol. Immunol. 24*, 151–161.
Wofsy, C., Goldstein, B., & Dembo, M. (1978) *J. Immunol. 121*, 593–601.
Yamakawa, H., & Fujii, M. (1973) *Macromolecules 6*, 407–415.
Yarmush, D. M., Morel, G., & Yarmush, M. L. (1987) *J. Biochem. Biophys. Methods 14*, 279–289.
Yarmush, D. M., Murphy, R. M., Colton, C. K., Fisch, M., & Yarmush, M. L. (1988) *Mol. Immunol. 25*, 17–25.

Induction of G·C to A·T Transitions by the Acridine Half-Mustard ICR-191 Supports a Mispairing Mechanism for Mutagenesis by Some Bulky Mutagens†

Sudhir R. Sahasrabudhe, Xun Luo, and M. Zafri Humayun*
Department of Microbiology and Molecular Genetics, University of Medicine and Dentistry of New Jersey–New Jersey Medical School, 185 South Orange Avenue, MSB F607, Newark, New Jersey 07103-2757
Received March 15, 1990; Revised Manuscript Received August 22, 1990

ABSTRACT: As the most nucleophilic atom in DNA, the guanine N7 atom is a major site of attack for a large number of chemical mutagens as well as chemotherapeutic agents. Paradoxically, while methylation of guanine N7 is believed to be largely nonmutagenic, aflatoxin B_1, among the most potent mutagens, appears to exert its mutagenic activity through adduction at this site. On the basis of an analysis of the specificity of mutations induced by various adduct forms of aflatoxin B_1, we have previously proposed mechanisms that can both resolve the paradox and account for the specificity of mutagenesis by aflatoxin B_1. The hypothesized mechanisms specify how a bulky guanine N7 lesion can promote G·C to A·T transitions as well as frame-shift mutations. Since the proposed mechanisms are in principle lesion-independent, a simple test of the proposed mechanisms would be to examine the specificity of mutations induced by a structurally different bulky guanine N7 adduct. Toward this goal, M13 replicative form DNA was subjected to in vitro adduction with the acridine mutagen ICR-191 and transfected into *Escherichia coli*. Mutations in the LacZ(α) gene segments were scored and defined at the sequence level. The results show that ICR-191 adduction induces both base substitutions and frame shifts with near-equal efficiency. A clear majority of base substitutions were G·C to A·T transitions. On the other hand, unlike aflatoxin B_1 which could induce both −1 and +1 frameshifts, ICR-191 appears to predominantly induce +1 frame shifts. This preference appears to arise by lesion-dependent mechanisms. The data presented in this communication are consistent with the proposed mechanisms for base substitution mutagenesis by bulky guanine N7 lesions and permit a further refinement of the previously proposed mechanisms for frame-shift induction by bulky DNA lesions.

Alkylating agents, which encompass a very broad range of laboratory mutagens and natural and man-made carcinogens as well as chemotherapeutic agents, are known to react with DNA predominantly at the guanine N7 position. On the other hand, the role of guanine N7 adduction in mutagenesis and carcinogenesis is poorly understood. For a long time, it has been thought that guanine N7 adduction may represent "tolerated" DNA damage which is neither lethal nor mutagenic, leading to a search for minor premutagenic lesions such as *O*-alkylated bases or lethal lesions such as cross-links. Experimental evidence on several O-alkylated bases has established that these lesions are indeed mutagenic [for brief reviews, see Basu and Essigmann (1988) and Walker (1984)].

† This work was supported by USPHS Grant CA27735.
* Corresponding author.

0006-2960/90/0429-10899$02.50/0